Journal of Alloys and Compounds 514 (2012) 150–156

Contents lists available at SciVerse ScienceDirect

Journal of Alloys and Compounds

journal homepage: www.elsevier.com/locate/jallcom

Synthesis and characterization of Ce–TZP/Al_2O_3 nanocomposites prepared via aqueous combustion

M. Asadirad*, H. Yoozbashizadeh

Department of Materials Science and Engineering, Sharif University of Technology, Azadi Ave., P.O. Box 11365-9466, Tehran, Iran

ARTICLE INFO

Article history:
Received 23 June 2011
Received in revised form 6 November 2011
Accepted 7 November 2011
Available online 17 November 2011

Keywords:
Aqueous combustion synthesis
Alumina–zirconia–ceria
Nanocomposites
Electron microscopy

ABSTRACT

Nanocomposites of Ce–TZP/Al_2O_3 were synthesized by aqueous combustion, and urea, ammonium acetate and glycine were used as mixtures of fuels with the corresponding metal nitrates. Thermodynamic modeling was conducted to anticipate the effect of the alumina content on the exothermicity of the combustion procedure. The thermodynamic properties of the combustion reaction indicated that as the alumina content increased, the amount of gases produced during the reaction increased with a decrease in the adiabatic temperature. Furthermore, to reduce the particle size of the powders, a series of combustion reactions were performed to optimize the fuel composition and alumina content. $Ce_{0.1}Zr_{0.9}O_2$–$0.80Al_2O_3$ nanocomposites prepared from 80 mol% alumina had a mean particle size of ~15 nm. Alternatively, samples containing 20 mol% alumina had a mean particle size of ~30 nm. X-ray diffractometry, transmission electron microscopy, scanning electron microscopy, and BET surface area analysis were conducted to characterize the powders.

1. Introduction

Ceramic–ceramic nanocomposites possess the advantages and properties of both ceramic materials and nanoparticles, including biocompatibility and high strength. Due to the presence of nanoscale particles and superior homogeneity, ceramic–ceramic nanocomposites display extraordinary electric, dielectric, magnetic, and optical properties, which are strongly affected by the particle size. Applications of these oxide ceramics include the manufacturing of cutting tools, dies and prosthetic components [1–9].

Ceria–tetragonal-zirconia-polycrystalline (Ce–TZP) nanocomposites are tetragonal polycrystalline materials [1]. Due to their biocompatibility and excellent mechanical properties and aesthetics, the manufacturing of nanoceramics, especially alumina–zirconia–yttria nanocomposites, has changed the field of orthopedic implant designs [2]. The high fracture toughness of Ce–TZP/Al_2O_3 nanocomposites may be superior to that of conventional Y–TZP (yttria-stabilized) in clinical applications. Although the flexure strength is equal to that of conventional Y–TZP, the fracture toughness of Ce–TZP/Al_2O_3 nanocomposites is significantly greater. By creating a homogeneous dispersion of nano-phased alumina in a TZP matrix, the mechanical properties and hydrothermal stability of tetragonal zirconia can be improved [3]. Zirconia particles expand the volume of the nanocomposite by 3–5%, which improves compressive stresses in the alumina matrix and inhibits cracking. Furthermore, zirconia particles associate and act as an energy barrier against crack growth and the destruction of the material [4]. Due to their mechanical properties and biocompatibility, Ce–TZP/Al_2O_3 nanocomposites are a promising material for biomedical applications [2].

In recent years, a significant amount of research has been conducted on the synthesis of zirconia-toughened-alumina (ZTA) nanocomposites. ZTA nanocomposites are usually synthesized by conventional ceramic techniques or methods based on co-precipitation or ball-milling. In conventional processes such as co-precipitation, various parameters such as the pH, temperature, concentration, stirring rate and dropping rate must be strictly controlled [1]. Compared to conventional methods, aqueous combustion synthesis (ACS) is distinct due to its versatility, simplicity and short ignition time. The unique specifications of ACS have led to the formation of a variety of nano-sized materials. Moreover, ACS can be used to produce a variety of oxide materials with ultrafine grains [10].

Over the last two decades, several investigations on the preparation of ZTA nanocomposites by ACS have been conducted. In these studies, the effects of the fuel mixture have been investigated [6,7,10,11]. The preparation of 10Ce–TZP/Al_2O_3 nanocomposites via aqueous combustion synthesis was investigated in the present study. The effect of the alumina content on the surface area of the powders was studied, and thermodynamic modeling was conducted to determine the behavior of the combustion reaction.

* Corresponding author. Tel.: +98 21 66165228; fax: +98 21 66005717.
E-mail address: mojtabaasadirad@alum.sharif.edu (M. Asadirad).

0925-8388/$ – see front matter © 2011 Elsevier B.V. All rights reserved.
doi:10.1016/j.jallcom.2011.11.029

2. Materials and methods

The following materials were used in the present study:

-Aluminum nitrate ($Al(NO_3)_3{\cdot}9H_2O$, Merck, >99.5%)	Oxidizer
-Cerous nitrate ($Ce(NO_3)_3{\cdot}6H_2O$, Merck, >99.5%)	Oxidizer
-Zirconyl nitrate ($ZrO(NO3)_2{\cdot}6H_2O$, Aldrich, 99.5%)	Oxidizer
-Ammonium nitrate (NH_4NO_3, Merck, >99.7%)	Oxidizer
-Glycine ($C_2H_5O_2N$, Merck, >99.7%)	Fuel
-Urea ($CO(NH_2)_2$, Acros, 99.5%)	Fuel
-Ammonium acetate (CH_3COONH_4, Merck, >99.7%)	Fuel
-Hexamethylenetetramine ($C_6H_{12}N_4$, Merck, >99.7%)	Fuel

Al_2O_3 nanocomposite powders were prepared by dissolving stoichiometric and non-stoichiometric amounts of aluminum nitrate and urea (U) and ammonium acetate (AA) and hexamethylenetetramine (HMT) in distilled water according to the proportions described in Table 1. The solutions were thoroughly stirred at room temperature until a homogenous mixture was obtained. The resulting aqueous solution was evaporated and burned at 450 °C in a muffle furnace.

Experiments were performed to optimize the conditions and exothermicity of the combustion reaction for the preparation of alumina by ACS and to decrease the grain size of the resulting powders.

2.1. Preparation of α-alumina

The type of fuel and fuel/aluminum nitrate ratio have a significant effect on the preparation of α-Al_2O_3 powders. Ionaş et al. [13] conducted a combustion reaction with a stoichiometric amount of U, and produced α-Al_2O_3 with a surface area of 24 m^2/g. The redox mixture was prepared by mixing a stoichiometric amount of aluminum nitrate with U and igniting at temperatures of 350–500 °C. Similarly, Kingsley and Patil [14] combusted a solution containing U and aluminum nitrate to produce solid Al_2O_3, and found that the aforementioned mixture boiled, produced a foam, evolved a significant amount of gases and burned with a glowing flame. In the present study, HMT, urea and ammonium acetate were combined and used as a fuel for the first time. During ACS, the exothermicity of mixtures containing HMT–metal nitrate complexes is high, and significant amounts of heat are generated for the formation of nano-sized oxides of zirconia, ceria and alumina [15]. An equal ratio of oxidizer and fuel is expressed in terms of the elemental stoichiometric coefficients [16]. According to the principles used in propellant chemistry, the oxidizing and reducing valancies of various oxidizers and fuels are considered as follows: C = 4, H = 1, O = −2, N = 0, Al = 3, etc. Therefore, the oxidizing valency of an oxidizer like $Al(NO_3)_3{\cdot}9H_2O$ becomes −15; and the reducing valency of glycine ($C_2H_5O_2N$) becomes +9.

Samples 4–12 were prepared using various ratios of U, AA and HMT, as illustrated in Table 1. Depending on the fuel and the type of metal ion, combustion can be described as flaming (gas phase) or non-flaming (smoldering and heterogeneous). Flaming reactions are attributed to the generation of gaseous products such as nitrogen oxides (NO_x) by metal nitrates and HNCO, NH_3 and CO, which are produced by the fuel. For instance, the aluminum nitrate–U reaction is highly exothermic ($T_{ad} \sim 1500$ °C) but does not explode due to the thermal insulating nature of alumina. Alternatively, transition metal nitrate–U reacts explosively. In contrast, AA fuel does not generate very high temperatures in combustion reactions. Therefore, to prevent sintering and reduce the exothermicity of the reaction, the amount of U in the fuel was reduced (samples 4–6). To optimize the fuel ratio, fuels such as AA or HMT were added to the mixture. Aruna and Rajam [6] reported that 0.75U–0.25AA had yielded alumina with reduced agglomeration, so this fuel composition was chosen in the present work. Except for fuel composition 0.75U–0.25AA, U and 0.75U–0.25HMT, all of the reactions were classified as smoldering. The experimental results revealed that the combustion reaction becomes smoldering as the AA content increases and the amount of U and HMT decreases.

The theoretical stoichiometric reactions for the formation of alumina can be described as follows:

$$2Al(NO_3)_3{\cdot}9H_2O + 5CO(NH_2)_2 \rightarrow Al_2O_3 + 5CO_2 + 8N_2 + 28H_2O \quad (1)$$

$$2Al(NO_3)_3{\cdot}9H_2O + 2.73CH_3COONH_4 \rightarrow Al_2O_3 + 5.46CO_2 + 4.36N_2 + 27.55H_2O \quad (2)$$

$$2Al(NO_3)_3{\cdot}9H_2O + 1.166C_6H_{12}N_4 \rightarrow Al_2O_3 + 5CO_2 + 5.333N_2 + 25H_2O \quad (3)$$

2.2. Preparation of 10Ce–ZTP/Al_2O_3

The synthesis of $xCe_{0.1}Zr_{0.9}O_2$–$(1-x)Al_2O_3$ nanocomposites was also evaluated. One of the most important objectives of the present study was to investigate the effect of the alumina content on the particle size of $xCe_{0.1}Zr_{0.9}O_2$–$(1-x)Al_2O_3$ nanocomposite powders. Cerium oxide was used as a stabilizer to stabilize zirconia. 10Ce–ZTP/Al_2O_3 was prepared from 0.75U–0.25AA and a stoichiometric amount of glycine (with respect to ZrO_2), and the smallest particle size of Al_2O_3 was observed. Glycine is an interesting complexing agent that is used to improve the solubility of the zirconyl ion in water [17]. Moreover, glycine acts as a controlling agent for combustion reactions by forming complexes with metal ions [16]. Thus, glycine was used as a fuel in the present study. Typically, glycine is observed in the combustion products, along with traces of carbon. Therefore, ammonium nitrate, which acts as an oxidizer, was added to the fuel. Ammonium nitrate is not combustible alone; however, as an oxidizing agent, it can assist in the combustion of other materials, even if air is excluded [18]. Various types of fuels affect the reaction temperature and the degree of crystallization of the final powder. As illustrated in Table 1, if the combustion temperature does not reach the crystallization temperature, an amorphous semi-decomposed precursor will be obtained. Alternatively, when the combustion temperature is high, the growth of particles is limited by the short reaction time, and turbulence caused by the evolution of gas during the reaction hinders the degree of agglomeration.

2.3. Characterization methods

To determine the crystallite size and phase of the combustion-synthesized α-Al_2O_3 and $xCe_{0.1}Zr_{0.9}O_2$–$(1-x)Al_2O_3$ powders, a Bruker Advance D8 X-ray diffractometer with Cu K_α ($\lambda = 0.154$ nm) radiation was employed. The average crystallite size was calculated according to the line broadening method. To determine the crystallite size (D) of the powders, PHILIPS X'Pert HighScore software was employed. A silicon disc was used as a standard to prevent instrumental broadening of the measured profiles. A substantial portion of the Scherrer equation is associated with structural broadening; thus, the following correction was applied:

$$B_{struct} = B_{obs} - B_{std} \quad (4)$$

where B_{obs} and B_{std} are the full width at half maximum (FWHM) of any reflection of the standard sample (silicon disc) and powder, respectively, and B_{struct} is the FWHM due to the crystallite size. Thus, the crystallite size was determined according to the Scherrer equation:

$$D = \frac{0.9\lambda}{\cos\ \theta\sqrt{B_{obs}^2 - B_{std}^2}} \quad (5)$$

where D is the crystallite size, λ is the wavelength of radiation, θ is Bragg's angle and B_{obs} and B_{std} are the FWHMs of the sample and standard material, respectively.

The size and morphology of the agglomerates were determined with a Cam-Scan MV 2300 scanning electron microscope. BET (Brunauer, Emmett and Teller) surface area measurements were performed using a Gemini 2375 V4.02 surface analyzer, and nitrogen was employed as the adsorption gas. Transmission electron microscopy (TEM) was performed with a CM200 FEG PHILIPS microscope operating at 200 kV to determine the shape and average size of the nanoparticles. Moreover, Microstructural Image Processing (MIP) software was used to determine the size of the agglomerates.

3. Results and discussion

3.1. Thermodynamic modeling

Sets of experiments were designed in a logical format to survey the effect of the alumina content on the particle size of $xCe_{0.1}Zr_{0.9}O_2$–$(1-x)Al_2O_3$ nanocomposites and to compare the exothermicity of different mole fractions of alumina in the aqueous combustion reaction and the enthalpy and adiabatic flame temperature of the reactions in the presence of urea, ammonium acetate, glycine, aluminum nitrate, zirconyl nitrate and cerous nitrate.

According to the combustion reactions shown in Eq. (6), the following products can be obtained by using stoichiometric amounts of reactants:

$$\begin{aligned}&(2-2x)\,Al(NO_3)_3.9H_2O + (x-xy)\,ZrO(NO_3)_2.6H_2O + xyCe(NO_3)_3.\\&6H_2O + CH_3COONH_4 +\\&CO(NH_2)_2 + C_2H_5O_2N + NH_4NO_3 + 4.5O_2 = xCe_yZr_{1-y}O_2\\&-(1-x)Al_2O_3 + 5CO_2 + (28-\\&12x)H_2O + (3+0.5x)N_2 + (6-5x+xy)NO_2\\&(\text{for all samples } y = 0.1)\end{aligned} \quad (6)$$

- $0.95Ce_{0.1}Zr_{0.9}O_2$–$0.05Al_2O_3$ ($x = 0.95$)
- $0.9Ce_{0.1}Zr_{0.9}O_2$–$0.1Al_2O_3$ ($x = 0.9$)
- $0.85Ce_{0.1}Zr_{0.9}O_2$–$0.15Al_2O_3$ ($x = 0.85$)
- $0.8Ce_{0.1}Zr_{0.9}O_2$–$0.2Al_2O_3$ ($x = 0.8$)
- $0.6Ce_{0.1}Zr_{0.9}O_2$–$0.4Al_2O_3$ ($x = 0.6$)
- $0.4Ce_{0.1}Zr_{0.9}O_2$–$0.6Al_2O_3$ ($x = 0.4$)
- $0.2Ce_{0.1}Zr_{0.9}O_2$–$0.8Al_2O_3$ ($x = 0.2$)

The heat of the reaction and the theoretical combustion temperature as a function of the mole fraction of Al_2O_3 in a $Ce_{0.1}Zr_{0.9}O_2$ solid solution was calculated using the thermodynamic data (which

Table 1
Properties of alumina prepared by aqueous combustion process using various fuel compositions.

Sample name	Fuel composition	Particle size from XRD (nm)	Agglomerate size from SEM (μm)
1	AA	Amorphous	–
2	HMT	Amorphous	–
3	U	48	11
4	0.75U–0.25AA	25	7
5	0.5U–0.5AA	Amorphous	–
6	0.25U–0.75AA	Amorphous	–
7	0.75HMT–0.25AA	Amorphous	–
8	0.5HMT–0.5AA	Amorphous	–
9	0.25HMT–0.75AA	Amorphous	–
10	0.75U–0.25HMT	40	10
11	0.5U–0.5HMT	Amorphous	–
12	0.25U–0.75HMT	Amorphous	–

AA, ammonium acetate; HMT, hexamethylenetetramine; U, urea.

Table 2
Relevant thermodynamic data.

Compound	Heat of formation at 298 K (kJ/mol)	C_p values (J/mol K)[a]
$ZrO(NO_3)_2$(c)	−1909.15	–
$Al(NO_3)_3{\cdot}9H_2O$(c)	−3590.55	–
$Ce(NO_3)_3$(c)	−1225.03	–
CH_3COONH_4(c)	−616.13	–
$CO(NH_2)_2$(c)	−235.68	–
$C_2H_5O_2N$(c)	−333	–
NH_4NO_3(c)	−365.4	–
$Ce_{0.1}Zr_{0.9}O_2$(c)	−1099.77	–
Al_2O_3(c)	−1674	$117.49+(10.38\times10^{-3}\times T)-(37.11\times10^{5}\times T^{-2})$
O_2(g)	0	$29.977+(4.1868\times10^{-3}\times T)-(1.6747\times10^{5}\times T^{-2})$
N_2(g)	0	$30.42+(2.54\times10^{-3}\times T)-(2.37\times10^{5}\times T^{-2})$
CO_2(g)	−393.77	$44.14+(9.04\times10^{-3}\times T)-(8.54\times10^{5}\times T^{-2})$
H_2O(g)	−242	$30+(10.718\times10^{-3}\times T)-(0.335\times10^{5}\times T^{-2})$
NO_2(g)	+33.1	$34.53+(24.67\times10^{-3}\times T)-(4.2\times10^{5}\times T^{-2})-(6.87\times10^{-6}\times T^{2})$

c, crystalline; g, gas; T, absolute temperature.
[a] Calculated from the discrete values.

were obtained from Table 2) shown in Table 3. The enthalpy and theoretical combustion temperature were calculated using the following expressions:

$$\Delta H = \left(\sum n\Delta H_p\right) - \left(\sum n\Delta H_r\right) = \int_{T_o}^{T_f} (\Delta n C_p)dT \quad (7)$$

T_f can be calculated from a heat balance equation:

$$|\Delta H^R| = \int_{T_o}^{T_f} \left(\sum C_p\right)_{\text{products}} dT \quad (8)$$

where ΔH_r and ΔH_p are the enthalpy of formation of the reactants and products, respectively, T_f is the adiabatic flame temperature, T_o is 298 K and C_p is the molar heat capacity of the products and reactants at a constant pressure.

The calculated enthalpy of combustion and the theoretical adiabatic flame temperature as a function of the alumina content are illustrated in Figs. 1 and 2, respectively. Reactions conducted with the lowest amount of alumina ($x = 0.95$) displayed the highest exothermicity and adiabatic flame temperature. Alternatively, the largest alumina content ($x = 0.2$) resulted in the lowest exothermicity and adiabatic flame temperature. Figs. 1 and 2 also revealed that the theoretical combustion temperature decreased with an increase in the alumina content. Similar results have been reported by Toniolo et al. [19], who calculated the enthalpy and theoretical flame temperature of the glycine–nitrate combustion synthesis of alumina. The theoretical combustion temperature decreased with an increase in the alumina content because the moles of gas released during combustion are directly proportional to the alumina content. Namely, gases produced during the reaction remove heat from the combustion zone, which results in a low theoretical combustion temperature. However, the actual flame temperature is always lower than the calculated value due to heat losses, incomplete combustion and additional air.

3.2. X-ray diffraction

The X-ray diffraction patterns of the alumina samples are illustrated in Fig. 3. The particles were crystalline, and the size of the

Table 3
The heat of combustion, T_{ad}, number of moles of gas and average crystallite size as a function of alumina content.

Compound	Heat of formation at 298 K (kJ/mol)	T_{ad} (K)	No. of moles of gas	Average crystallite size using XRD (nm)
$Ce_{0.1}Zr_{0.9}O_2$–0.05Al_2O_3	−2092	2824	20.72	24
$Ce_{0.1}Zr_{0.9}O_2$–0.10Al_2O_3	−2387	2813	21.84	21
$Ce_{0.1}Zr_{0.9}O_2$–0.15Al_2O_3	−2567	2797	22.96	19
$Ce_{0.1}Zr_{0.9}O_2$–0.20Al_2O_3	−2713	2777	24.08	17
$Ce_{0.1}Zr_{0.9}O_2$–0.40Al_2O_3	−3365	2746	28.56	15
$Ce_{0.1}Zr_{0.9}O_2$–0.60Al_2O_3	−4017	2736	33.04	13
$Ce_{0.1}Zr_{0.9}O_2$–0.80Al_2O_3	−4669	2725	37.52	10
Al_2O_3	−5322	2712	42	–

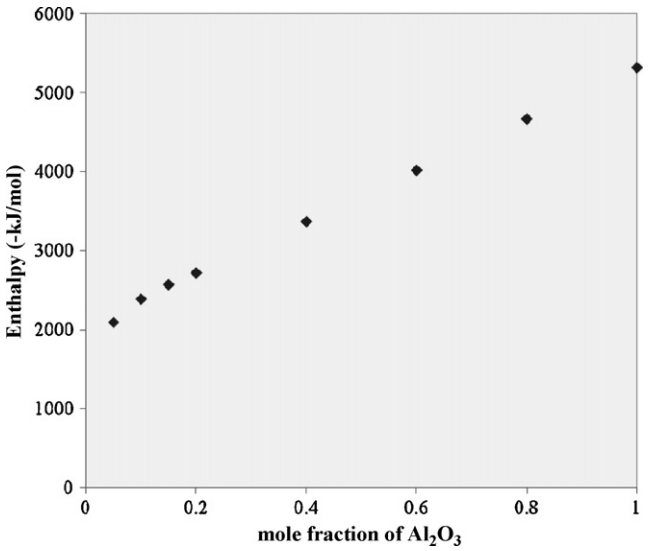

Fig. 1. Enthalpy as a function of the alumina content.

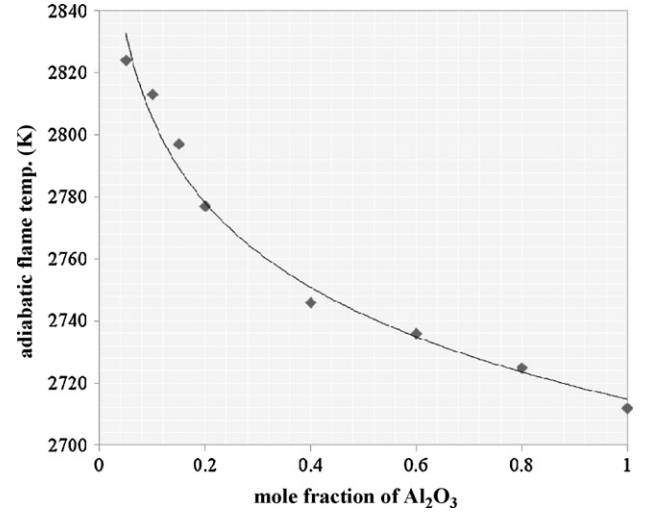

Fig. 2. Adiabatic flame temperature as a function of the alumina content.

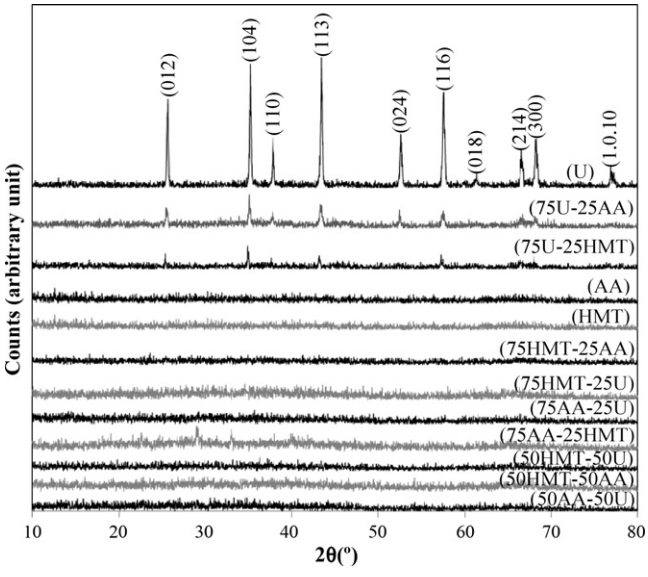

Fig. 3. XRD patterns of alumina powders.

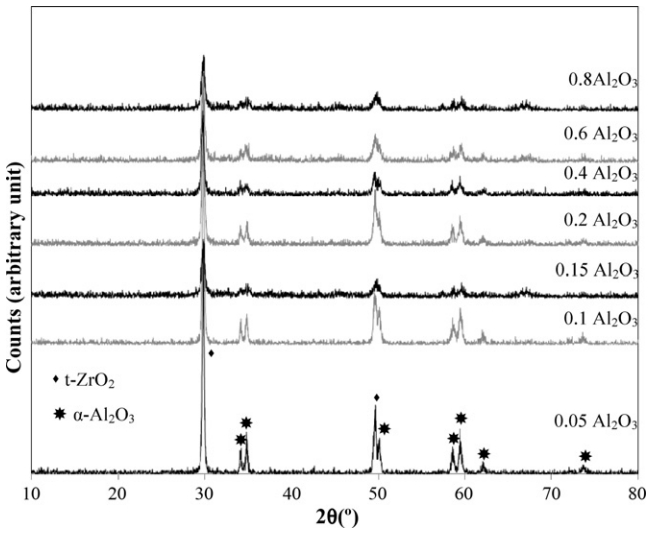

Fig. 4. XRD pattern of $xCe_{0.1}Zr_{0.9}O_2$–$(1-x)Al_2O_3$ (x = 0.95, 0.9, 0.85, 0.8, 0.6, 0.4 and 0.2) nanocomposites.

crystallites calculated from the XRD results of samples 3, 4, and 10 were 48, 25 and 40 nm, respectively. As shown in the figure, an amorphous phase was observed in the majority of the samples, except for powders synthesized from U, 0.75U–0.25AA and 0.75U–0.25HMT. In the sample synthesized from 0.75U–0.25AA, the powders contained a well-crystallized α-Al_2O_3 phase with relatively broad peaks. Several combustion reactions using the fuel ratios shown in Table 1 were performed, and the results showed that the characteristic XRD peaks became thinner and stronger as the AA content decreased and the U content increased. The optimal amount of fuel for the production of nanocrystalline alumina with reduced agglomeration was 0.75U–0.25AA. Similar results have been reported by Aruna and Rajam [6], who used AA to modify U-based fuel for the synthesis of α-alumina particles with small crystallites. Therefore, to prepare 10Ce–TZP/Al_2O_3, 0.75U–0.25AA and a combination of fuels containing glycine and ammonium nitrate were employed. Binary fuels containing 75U–25AA produced broader and weaker peaks due to a reduction in the exothermicity of the combustion reaction, as reported in the literature [6,10]. Results show that the new combination of fuels like 0.75U–0.25HMT has not yielded lower grain sized alumina compared to 0.75U + 0.25AA. Thus, it can be concluded that the AA acts more effective rather than HMT in the same composition.

The X-ray diffraction patterns of 10Ce–TZP/Al_2O_3 with different amounts of alumina are shown in Fig. 4. 10Ce–TZP/Al_2O_3 powder exhibited broad peaks, confirming the nano-size nature of the material. Broad peaks were also observed in $Ce_{0.1}Zr_{0.9}O_2$–$0.05Al_2O_3$ and α-alumina, and zirconia peaks were not detected. The XRD pattern was indicative of an amorphous phase; thus, the resulting fine powders were calcined at room temperature to 500 °C for 1 h and 40 min, 500 °C for 2 h, 500–1150 °C for 2 h and 10 min and 1150 °C for 2 h.

The average crystallite sizes of ZrO_2 and Al_2O_3 particles calculated from the Debye–Scherrer equation were 11 and 9 nm, respectively, for $Ce_{0.1}Zr_{0.9}O_2$–$0.80Al_2O_3$. The crystallite size of 10Ce–TZP/Al_2O_3 nanocomposites as a function of the theoretical combustion temperature is shown in Table 2. As shown in the table, the average crystallite size (calculated from XRD) of alumina–zirconia–ceria nanocomposites containing 5 and 80 mol% Al_2O_3 was 24 and 10 nm, respectively. As the alumina content increased, the crystallite size of 10Ce–TZP/Al_2O_3 nanocomposites decreased because the theoretical combustion temperature

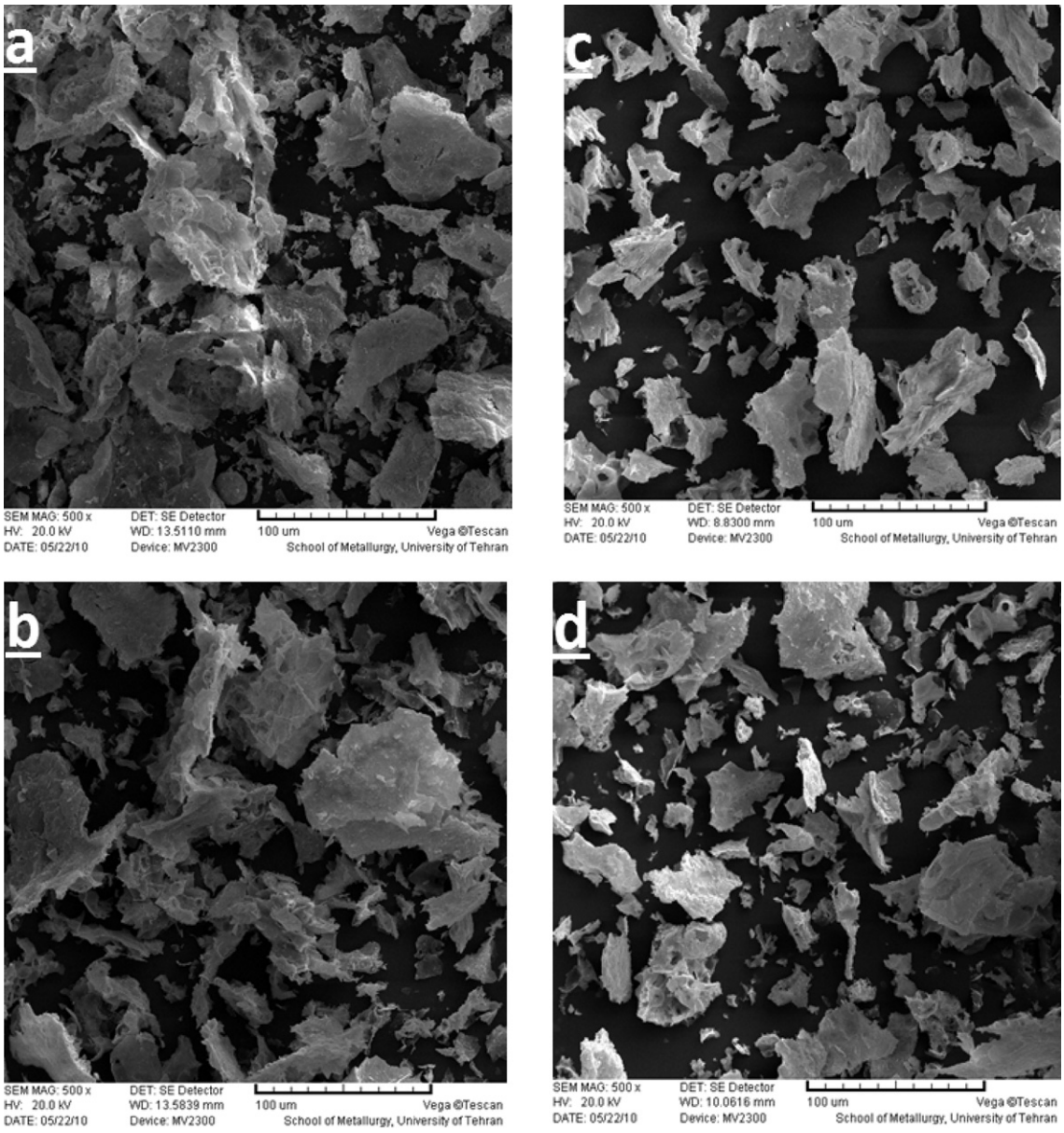

Fig. 5. Scanning electron micrographs of 10Ce–TZP/Al_2O_3 nanocomposite powders: (a) $Ce_{0.1}Zr_{0.9}O_2$–0.20Al_2O_3, (b) $Ce_{0.1}Zr_{0.9}O_2$–0.40Al_2O_3, (c) $Ce_{0.1}Zr_{0.9}O_2$–0.60Al_2O_3, (d) $Ce_{0.1}Zr_{0.9}O_2$–0.80Al_2O_3.

decreased from 2551 °C for $Ce_{0.1}Zr_{0.9}O_2$–0.05Al_2O_3 to 2439 °C for $Ce_{0.1}Zr_{0.9}O_2$–0.80Al_2O_3, which retarded crystal growth.

3.3. Scanning electron microscopy (SEM)

SEM was used to determine the morphology of the agglomerates of 10Ce–TZP/Al_2O_3 nanocomposite powders. The SEM of nanocomposite powders with different alumina contents is shown in Fig. 5. In these samples, the agglomerated particles were smaller than those of ZTA ceramics [6,7,10]. For all of the samples, the micrographs exhibited flaky agglomerated particles and several pores in their structures, which were attributed to the evolution of a large amount of gas during combustion. Furthermore, the size of the pores increased with an increase in the alumina content of the 10Ce–TZP/Al_2O_3 nanocomposite powders due to an increase in the moles of gas. Namely, the evolution of gas caused the agglomerates to break up, which increased the porosity of the material.

3.4. BET analysis

The BET surface area results are illustrated in Table 4. The specific surface area of the powders increased from 7 to 17.1 m^2/g for nanocomposites containing 5 and 80 mol% Al_2O_3, respectively. The maximum value obtained in the present study (17.1 m^2/g) is significantly greater than that of a ZTA sample produced from 0.75U–0.25AA (13.16 m^2/g) by Tahmasebi and Paydar [12]. The high surface area of the nanocomposite produced in the present investigation (17.1 m^2/g) can be attributed to the use of ceria as a stabilizer or the application of a single fuel during the preparation of 10Ce–TZP/Al_2O_3. Moreover, increasing the alumina content decreased the adiabatic flame temperature of the combustion reaction and limited the agglomeration of particles, which increased the specific surface area. The grain size, D_{BET}, was also calculated using Eq. (9) [20].

$$D_{BET} = \frac{6000}{\rho \times S_{BET}} \quad (9)$$

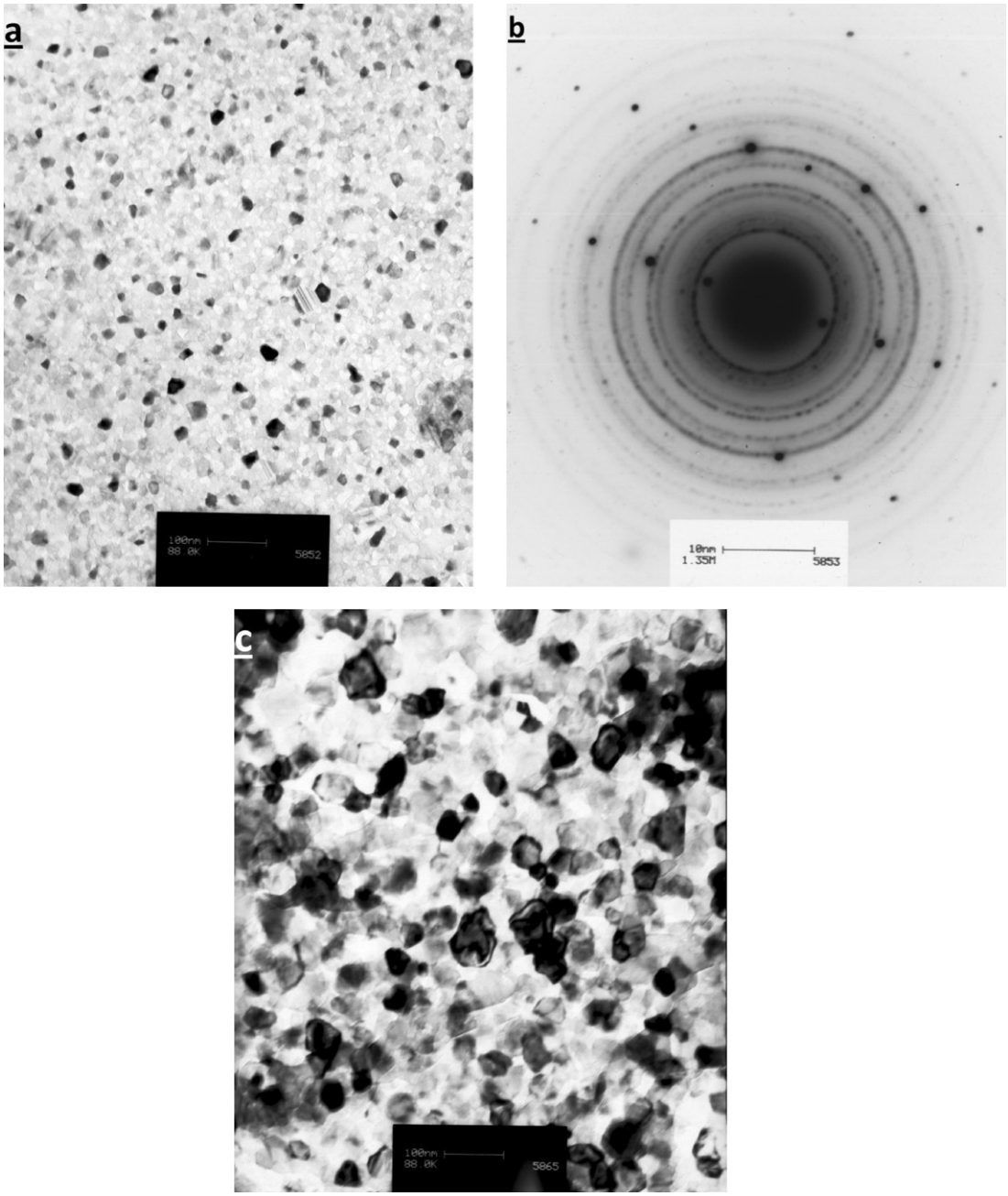

Fig. 6. Transmission electron micrographs of 10Ce–TZP/Al_2O_3 nanocomposite powders: (a) 0.2$Ce_{0.1}Zr_{0.9}O_2$–0.80Al_2O_3 nanoparticles, (b) selected area electron diffraction pattern, (c) $Ce_{0.1}Zr_{0.9}O_2$–0.20Al_2O_3 nanoparticles.

Table 4
Properties of powder prepared using different alumina content.

Compound	Crystalline size using XRD (nm)		Particle size using TEM (nm)		Agglomerate size using SEM (μm)	Specific surface area (m^2/g)
	Al_2O_3	ZrO_2	Al_2O_3	ZrO_2		
$Ce_{0.1}Zr_{0.9}O_2$–0.05Al_2O_3	18	29	–	–	28	7
$Ce_{0.1}Zr_{0.9}O_2$–0.10Al_2O_3	17	25	–	–	26	9
$Ce_{0.1}Zr_{0.9}O_2$–0.15Al_2O_3	16	23	–	–	23	11.2
$Ce_{0.1}Zr_{0.9}O_2$–0.20Al_2O_3	15	19	26	35	20	14.5
$Ce_{0.1}Zr_{0.9}O_2$–0.40Al_2O_3	12	17	–	–	15	15.1
$Ce_{0.1}Zr_{0.9}O_2$–0.60Al_2O_3	11	15	–	–	13	16.3
$Ce_{0.1}Zr_{0.9}O_2$–0.80Al_2O_3	9	11	12	18	10	17.1

where D_{BET} is the grain size (nm), ρ is the theoretical density of 10Ce–TZP/Al_2O_3 and S_{BET} is the surface area (m^2/g). The grain size (D_{BET}) and crystallite size (D_{XRD}) of $Ce_{0.1}Zr_{0.9}O_2$–0.05Al_2O_3 were calculated, and values of 140 and 24 nm were obtained, respectively. The observed difference between D_{BET} and D_{XRD} indicated that each grain contained a large number of crystallites and suggested that the crystallites were highly agglomerated.

3.5. Transmission electron microscopy (TEM)

TEM micrographs of samples containing 20 and 80 mol% Al_2O_3 are shown in Fig. 6. In the TEM micrographs, alumina and zirconia appear as bright and dark phases, respectively. The zirconia particles were distinctively uniform and homogeneously distributed throughout the matrix, as evidenced in the micrographs. The results obtained from MIP software showed that the mean diameter of Al_2O_3 in $Ce_{0.1}Zr_{0.9}O_2$–0.80Al_2O_3 and $Ce_{0.1}Zr_{0.9}O_2$–0.20Al_2O_3 was 26 and 12 nm and that the mean diameter of ZrO_2 was 35 and 18 nm, respectively. The TEM images confirmed the results obtained from the XRD patterns, which suggested that the fuel composition has a significant effect on the size, shape and agglomeration of 10Ce–TZP/Al_2O_3 particles obtained via aqueous combustion. In addition, the particle sizes measured by TEM were slightly larger than those obtained by XRD. The observed difference between the sizes calculated by XRD and TEM may be due to the formation of nanocomposites and the fact that the crystalline phase powders were composed of crystallites.

4. Conclusions

In the present study, alumina–zirconia–ceria nanocomposite powders were synthesized via aqueous combustion. The optimal fuel composition for the preparation of 10Ce–TZP/Al_2O_3 was determined by performing a series of experiments. The nanocrystalline structure of α-alumina and t-zirconia powders was observed by XRD and TEM. As evidenced by XRD and BET, the particle size of 10Ce–TZP/Al_2O_3 nanocomposites could be altered by modifying the alumina content. $Ce_{0.1}Zr_{0.9}O_2$–0.20Al_2O_3 nanocomposites prepared from 20 mol% alumina had a particle size of ~30 nm and a surface area of 14.5 m^2/g. Alternatively, $Ce_{0.1}Zr_{0.9}O_2$–0.80Al_2O_3 prepared using 80 mol% alumina had a surface area of 17.1 m^2/g and a particle size of ~15 nm. Thus, as the alumina content increased, the exothermicity of the combustion reaction and the particle size of the powder decreased.

Acknowledgements

M.A and H.Y thank the Deputy of Research and Technology Grants and the Department of Materials Science and Engineering at Sharif University of Technology. The financial assistance received from the Iranian Nanotechnology Initiative Council is duly acknowledged.

References

[1] S.T. Aruna, K.C. Patil, Acta Metall. Nanostruct. Mater. 10 (1998) 955–964.
[2] R. Benzaid, J. Chevalier, M. Saâdaoui, G. Fantozzi, M. Nawa, L.A. Diaz, R. Torrecillas, Biomaterials 29 (2008) 3636–3641.
[3] J. Fischer, B. Stawarczyk, Dent. Mater. 23 (2007) 1500–1505.
[4] S. Biamino, P. Fino, M. Pavese, C. Badini, Ceram. Int. 32 (2006) 509–513.
[5] J. Fischer, B. Stawarczyk, A. Trottmann, C.H.F. Hämmerle, Dent. Mater. 25 (2009) 326–330.
[6] S.T. Aruna, K.S. Rajam, Mater. Res. Bull. 39 (2004) 157–167.
[7] J. Kishan, V. Mangam, B.S.B. Reddy, S. Das, K. Das, J. Alloys Compd. 490 (2010) 631–636.
[8] B.S.B. Reddy, I. Mal, S. Tewari, K. Das, S. Das, Metall. Mater. Trans. A 38A (2007) 1786–1793.
[9] P.M. Kelly, L.R.F. Rose, Prog. Mater. Sci. 47 (2002) 463–557.
[10] S.T. Aruna, A.S. Mukasyan, Curr. Opin. Solid State Mater. Sci. 12 (2008) 44–50.
[11] N.A. Dhas, K.C. Patil, Ceram. Int. 20 (1994) 57–66.
[12] K. Tahmasebi, M.H. Paydar, Mater. Chem. Phys. 109 (2008) 156–163.
[13] R. Ianoş, I. Lazău, C. Păcurariu, J. Mater. Sci. 44 (2009) 1016–1023.
[14] J.J. Kingsley, K.C. Patil, Mater. Lett. 6 (1988) 427–432.
[15] A.S. Prakash, A.M.A. Khadar, K.C. Patil, M.S. Hegde, J. Mater. Synth. Process. 10 (2002) 135–141.
[16] K.C. Patil, M.S. Hegde, T. Rattan, S.T. Aruna, Chemistry of Nanocrystalline Oxide Materials Combustion Synthesis, Properties and Applications, 1st ed., World Scientific, Singapore, 2008.
[17] I. Kaus, P.I. Dahl, J. Mastin, T. Grande, M. Einarsrud, J. Nanomater. 2006 (2006) 1–7.
[18] H.F. Mark, J.J. Mcketta Jr., D.F. Othmer (Eds.), Kirk-Othmer Encyclopedia of Chemical Technology, vol. 2, Interscience, New York, 1967.
[19] J.C. Toniolo, M.D. Lima, A.S. Takimi, C.P. Bergmann, Mater. Res. Bull. 40 (2005) 561–567.
[20] R. Ianoş, P. Barvinschi, J. Solid State Chem. 183 (2010) 491–496.